

**RESEARCH ARTICLE**

# Flipped detection of psychoactive substances in complex mixtures using handheld Raman spectroscopy coupled to chemometrics

Jesus Calvo-Castro<sup>1</sup>  | Steve N. Tchakounte<sup>1</sup> | Valentina Guarino<sup>2</sup> |  
Adeel A. Ahmed<sup>1</sup>  | Jacqueline L. Stair<sup>1</sup>

<sup>1</sup>School of Life and Medical Sciences,  
University of Hertfordshire, Hatfield

<sup>2</sup>Wythenshawe Hospital, Manchester, UK

**Correspondence**

Jesus Calvo-Castro and Jacqueline  
L. Stair, School of Life and Medical  
Sciences, University of Hertfordshire,  
Hatfield, AL10 9AB, UK.

Email: [j.calvo-castro@herts.ac.uk](mailto:j.calvo-castro@herts.ac.uk) and  
[j.stair@herts.ac.uk](mailto:j.stair@herts.ac.uk)

**Funding information**

Analytical Chemistry Trust Fund, Grant/  
Award Number: ACSS 17/025; European  
Commission, Grant/Award Numbers:  
JUST/2013/DPIP/AG/4823, JUST/ISEC/  
DRUGS/AG/6428

**Abstract**

New psychoactive substance (NPS) misuse represents a critical social and health problem. Herein, a novel flipped approach is presented for the detection of psychoactive substances in complex mixtures using portable Raman spectroscopy. This consists firstly of evaluating the spectral dissimilarities of an NPS product to its constituent adulterants followed by detection of the NPS by means of key spectral signatures. To demonstrate it, three structurally diverse NPS and four commonly used adulterants were selected. A Design-of-Experiments guided approach was employed to determine the composition of simulate street samples, ranging from binary to quinary mixtures of varying concentrations. Spectra were acquired for all mixtures using a portable Raman spectrometer and examined using projection analysis on model systems, developed via principal component analysis using reference materials. For all 21 mixtures investigated, the innovative ‘flipped’ methodology resulted in isolated and unequivocal detection of the NPS. Interestingly, the NPS signatures were consistent across all mixtures investigated and were 1712, 1000, and 777/1022  $\text{cm}^{-1}$  for 5F-PB-22, phenibut, and N-Me-2-AI containing samples, respectively. Thus indicating that the developed model systems could be applicable to structural analogs. NPS were detected to concentrations as low as 6.0% w/w. This flipped methodology was benchmarked to the instrument’s output algorithms and outperformed these in terms of NPS detection, particularly for low concentration ternary and quinary mixtures. As a result, this study represents a critical change in the conceptualization of novel approaches for the detection of psychoactive substances and further denotes a blueprint for the development of detection methodologies of target analytes in complex mixtures.

This is an open access article under the terms of the [Creative Commons Attribution-NonCommercial-NoDerivs](https://creativecommons.org/licenses/by-nc-nd/4.0/) License, which permits use and distribution in any medium, provided the original work is properly cited, the use is non-commercial and no modifications or adaptations are made.

© 2022 The Authors. *Journal of Raman Spectroscopy* published by John Wiley & Sons Ltd.

**KEYWORDS**

chemometrics, complex mixtures, design-of-experiments, new psychoactive substances (NPS), Raman spectroscopy

**1 | INTRODUCTION**

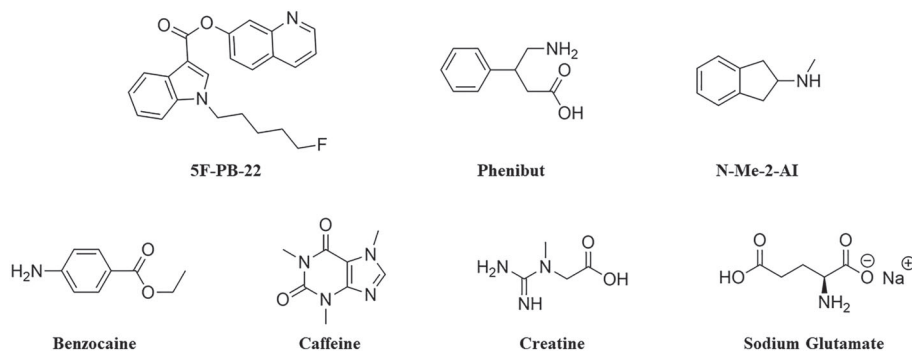
The growing number of new psychoactive substances (NPSs) that are available is a global challenge in terms of health, security, and monitoring. NPSs also commonly called “designer drugs” or “legal highs” are substances initially synthesized for the purpose of reproducing the psychoactive effect of controlled recreational drugs (e.g., ecstasy and cannabis) while bypassing existing legislation.<sup>[1]</sup> Approximately 50 unique NPSs are reported to the United Nations Office on Drugs and Crime (UNODC) each year, where a total of 1004 NPSs were recognized at the global level in October 2020.<sup>[2]</sup> It is widely reported that abuse of these substances often leads to negative outcomes such as violence and aggression, sympathomimetic effects, acute organ failures as well as fatalities.<sup>[3–6]</sup> This is compounded by the fact that still little is known about the acute and chronic health effects for such a diverse range of substances, and thus, targeted treatments are continually lagging behind. In recent years, as a means to decrease the abuse of NPS, many nations such as the United Kingdom and New Zealand have instated blanket bans to more extensively control these substances.<sup>[7,8]</sup> However, an increase in the control status requires tailored analytical methods that are capable of monitoring the sheer number and inherent chemical diversity of NPS and their products (Figure 1).

Consequently, law enforcement and health care organizations face a real challenge for the realization of efficient screening and identification analytical methodologies of NPS. This is exacerbated by the number of substances on the market growing at a continuum fast pace, where these emerging psychoactive substances range from having only a subtle chemical modification (i.e., chemical analogs) to those previously reported to unexpected new scaffolds. It is of note that the former represents a much more widely used approach when compared with the latter. In addition, remaining impurities as well as cutting agents and adulterants, added to bulk out the drug and/or provide some additional pharmacological effect, add to this chemical complexity and can often inhibit drug detection.<sup>[9–11]</sup> Interestingly, for the purpose of the work presented herein and unlike the case described for psychoactive substances, the development and utilization of novel cutting agents and adulterants is negligible. The gold standard for the identification of known NPS is lab-based analytical techniques such as

liquid and gas chromatographic techniques (LC and GC) coupled with mass spectrometry (MS) due to their accuracy and sensitivity.<sup>[4,12,13]</sup> Moreover, LC–MS is often applied for the analysis of biological fluids such as blood or urine (i.e., aqueous based), while GC–MS is more convenient in the analysis of tablets, capsules and powders (i.e., preparation via solvent extraction).<sup>[4,12]</sup> The latter requires solvent dissolution which can also reduce the impact from the cutting agents/adulterants enabling identification. In both cases, sending NPS samples to forensic laboratories can be costly and time-consuming resulting in only a selection of samples being analyzed. In recent years, there is a pressing need to have an initial identification (i.e., first pass) of suspect NPS samples where they are originally encountered (e.g., border control, prison, field policing, and health clinics).<sup>[12,14–16]</sup> It should be noted that the use of chromatographic approaches represents the gold standard for the identification of known NPS, while the identification of suspected novel analogs requires the utilization of other techniques such as NMR spectroscopy.<sup>[17–19]</sup>

Handheld spectroscopic instrumentation is of particular interest for rapid NPS detection due to their ease of use and quick response, which is facilitated by correlations of the unknown substance to on-board spectral libraries.<sup>[20–26]</sup> A comparative analysis between handheld IR, NIR, and Raman spectroscopies showed Raman as a more promising technique in the identification of NPS in mixtures due to numerous sharp analyte peaks as well as an insensitivity to polar functional groups (e.g., -OH and -HN).<sup>[27]</sup> Additionally, Raman spectroscopy has the advantage of minimal to no sample preparation and through-package analysis. For this reason, it has been used successfully over the years for traditional drugs of abuse (e.g., cocaine, heroin, and methamphetamine) and more recently for discrimination of NPS classes with principal component analysis (PCA).<sup>[20–23]</sup> Yet, one main obstacle that remains is the impact of the NPS product matrix (i.e., impurities, cutting agents, and adulterants) on the Raman spectra and how to overcome this for improved drug identification.<sup>[20,21,24,25,27,28]</sup> The matrix can impact on NPS identification in the following key ways: (1) The presence of fluorescence from the matrix can swamp the Raman signal, and more importantly, (2) the matrix can dilute and/or interfere with the spectral signals of the NPS. While the effect of fluorescence can be reduced or in many cases eliminated by

**FIGURE 1** Chemical structures for the three new psychoactive substance (NPS) and four adulterants used in this study



employing a lower-energy excitation source (e.g., 1064 nm)<sup>[21,25,29]</sup>, the complications posed by commonly used adulterants such as benzocaine, lidocaine, caffeine and procaine in products as well as inert components such as talc and cellulose for powder bulk still represent a critical problem that needs addressing in the development of Point-of-Use detection methodologies. In the case of spectroscopic approaches, this is particularly aggravated by the inferior resolution and signal-to-noise ratio (S/N) of handheld Raman instrumentation when compared with lab-based equipment. Along these lines, there is limited understanding as to what extent NPS identification is hindered by cutting agents, adulterants, or the presence of structurally similar substances in regard to dilution and spectral interference. A number of studies have reported on issues of identification with specific NPS samples due to the matrix with handheld Raman spectroscopy,<sup>[23,25,27,28]</sup> but these are on a case-by-case basis and do not represent a blueprint for the development of superior technologies. Recent guidance from the UNODC recommends evaluation for matrix interference as a key validation parameter for drug identification using handheld Raman spectrometers; however, this is left for the user to determine.<sup>[30]</sup> Although evaluation of “real-life” samples is crucial to determine the usefulness of an analytical technology, the literature lacks cohesiveness which would allow examination of trends and development of criteria useful for interpretation of key aspects. Thus, comprehensive insight and a more systematic approach are needed to succinctly inform guidance and advice for NPS identification using handheld Raman spectroscopy.

Motivated by these shortcomings, herein we present an innovative approach for the unequivocal detection of psychoactive substances in complex mixtures by means of handheld Raman spectroscopy coupled to chemometrics. While approaches based on spectroscopic techniques and chemometrics have been previously described, these largely rely on the spectral similarities between target analytes and NPS reference standard materials, attributing successful identification to their

relative orientation in two- and three-dimensional scores plots.<sup>[20,23,29,31]</sup> Uniquely, unlike NPS, the toolbox of substances commonly used as adulterants and cutting agents remains constant, allowing for a detailed understanding of their spectral properties. As a result, in this work, a reversal of the traditional approaches is proposed, a so-called flipped detection. It is hypothesized that to facilitate the rapid in situ detection of psychoactive substances in complex mixtures, the rationale should be on the dissimilarities between NPS and adulterants/cutting agents rather than similarities to NPS reference standards in available libraries, which often leads to challenges in the detection of the target analyte due to observed low correlations. Firstly, the presence of a potential psychoactive substance in a mixture is highlighted by its dissimilarity to cutting agents and adulterants, thus, bypassing the complications highlighted for currently used methods such as the lack of updated libraries for reference materials and/or poor spectral intensities. Next, the unequivocal detection of the target analyte is facilitated by key Raman active bands. It is anticipated that this approach will allow for the successful detection of chemical analogs (vide supra) characterized by negligible differences in their spectral signatures, that is, target spectral features belonging to classes and subclasses of psychoactive substances and not individual representatives.<sup>[32]</sup>

## 2 | EXPERIMENTAL SECTION

### 2.1 | NPS and adulterants used in the study

High purity ( $\geq 97\%$ ) NPS reference standards (10 mg) were purchased from Chiron Pharmaceuticals Limited (Bristol, UK) for the creation of Raman reference spectra. A larger quantity of NPS was required to generate the powder mixtures; thus, a set of NPS were purchased from UK online suppliers in February 2016 under Home Office license. The identity and purity were evaluated (SI.1) using gas chromatography mass spectroscopy (GC-MS)

TABLE 1 Composition of the test samples generated using the DoE-guided approach in this work

Test sample (TS)	Composition/mg				
	NPS	Benzocaine	Caffeine	Creatine	Sodium glutamate
1	150	0	0	0	0
2	10	0	140	0	0
3	10	140	0	0	0
4	10	0	0	140	0
5	10	0	0	0	140
6	80	0	70	0	0
7	80	70	0	0	0
8	80	0	0	70	0
9	80	0	0	0	70
10	10	70	70	0	0
11	10	0	70	70	0
12	10	0	70	0	70
13	10	70	0	70	0
14	10	70	0	0	70
15	10	0	0	70	70
16	94	14	14	14	14
17	24	14	84	14	14
18	24	84	14	14	14
19	24	14	14	84	14
20	24	14	14	14	84
21	38	28	28	28	28

Note: NPS = 5F-PB-22, phenibut or N-Me-2-AI.

Abbreviations: DoE, Design-of-Experiments; NPS, new psychoactive substance.

and high-performance liquid chromatography (HPLC). The purity was determined to be  $90.2 \pm 0.8$ ,  $95.4 \pm 0.4$ , and  $99.6 \pm 0.1\%$  for 5F-PB-22, phenibut, and N-ME-2-AI, respectively. Adulterants were all purchased from Sigma Aldrich (Dorset, UK) and used as received.

## 2.2 | Generation of complex mixtures (test samples [TS]) using selected NPS and adulterants

A DoE-guided approach was used to generate a smaller number of NPS mixtures to represent the complexity of one NPS combined with up to four adulterants. A simplex algorithm was applied with a quadratic fit where the total mixture mass was set to 150 mg; at least 10 mg of NPS was present in every combination investigated, and the adulterants ranged between 0 and 140 mg. The DoE approach resulted in 21 diverse compositions ranging from pure NPS to quinary mixtures (Table 1). These will be referred to as TS 1–21.

## 2.3 | Handheld Raman spectroscopy

A Progeny handheld Raman spectrometer (Rigaku, USA) was selected for the study based on previous reports for NPS detection.<sup>[21,23,29]</sup> The spectrometer had an excitation wavelength of 1064 nm coupled to a TE cooled InGaAs detector (512 pixels). The handheld instrument had a weight of 1.6 kg, dimensions of 29.9 cm × 8.1 cm × 7.4 cm, a theoretical battery life of over 5 h, and an optimum operating temperature range of  $-20^{\circ}\text{C}$  to  $50^{\circ}\text{C}$ . The instrument had an adjustable laser power of 30–490 mW, exposure time ranging from 5 ms to 30 s, and a spectral range of 200–2500  $\text{cm}^{-1}$  with a resolution of 8–11  $\text{cm}^{-1}$ . The instrument was calibrated daily using a benzonitrile reference standard (Rigaku, USA). Measurements were made using the baseline correction, 200 (for 5F-PB-22 and N-Me-2-AI containing samples) or 350 (for phenibut-containing samples) mW laser power, 2000 ms exposure time, and 10 acquisitions. In most cases, analysis was conducted through glass vials (Kimble Chase vial screw PTFE cap, China) using the

vial attachment; however, for the NPS reference compounds (<10 mg), spectra were collected on aluminum plates.<sup>[20,21]</sup> Raman spectra of the reference standards were collected and added to an in-house NPS-related spectral library on board the instrument (99 compounds). Raman spectra of the TS, with DoE-generated compositions (Table 1), were collected ( $n = 4$ ); vials were vortex mixed using a Vortex-Genie 2 (Scientific industries Inc., USA) for 1 min before the first run and 30 s between replicates to obtain a representative result. A thorough and comprehensive evaluation of each TS via the spectrometer's in-built algorithms is presented in the supporting information (SI.4).

## 2.4 | Hierarchical clustering and PCA

Experimentally acquired Raman spectra ( $n = 10$ ) for reference standards of NPS and adulterants were initially critically evaluated using clustering analysis by means of hierarchical complete linkage method and absolute correlation, as implemented in the Unscrambler X 10.5.1 software (CAMO, Oslo, Norway). Model systems containing one NPS and all four adulterants ( $n = 10$ ) were developed by means of PCA, employing NIPALS (Nonlinear Iterative Projection by Alternating Least Squares) algorithm as implemented in the Unscrambler X 10.5.1 software (CAMO, Oslo, Norway) and full cross validated (one sample per segment). To evaluate the feasibility of the proposed flipped detection approach, simulated street samples (Table 1) were tested against their respective model systems by means of projection PCA, using average spectra ( $n = 4$ ). The proposed methodology is based on a two-step process, whereby both Steps work alongside each other rather than independently. Step 1 explores the dissimilarities of the analyzed sample with respect to reference spectra for adulterants instead of similarities to those of NPS reference standard materials. This is then followed by, Step 2, the confirmation of the presence of the NPS by judicious evaluation of key spectral signatures, which are unique to NPS and therefore absent from the spectra of adulterants. In all cases, raw Raman spectra were then used to allow for direct performance comparison with respect to instrument's in-built algorithms; again, a comprehensive evaluation of this is presented in the supporting information (SI.4).

## 2.5 | Computational details

The unconstrained geometries of all three NPS and four adulterants were optimized (SI.2) by means of B3LYP density functional<sup>[33–35]</sup> at the 6-311G(d) level, as

implemented in Spartan 18 (v. 1.4.4) software.<sup>[36]</sup> In all cases, optimized geometries were confirmed by IR analyses, characterized by the absence of imaginary modes which denotes true equilibria minima.<sup>[37,38]</sup> Harmonic frequencies and Raman intensities were computed for these optimized geometries at the same level of theory, with observed scaling factors in line with those reported previously.<sup>[39]</sup> These computed harmonic frequencies were employed in the interpretation of the Raman spectral profiles of the reference standard materials of the selected NPS and adulterants for this work.

## 3 | RESULTS AND DISCUSSION

Thus, in this study the proposed 'flipped' methodology will be judiciously evaluated using a systematic approach guided by Design-of-Experiments (DoE) to generate simulated street mixtures. In this way, the known chemical composition will be used to inform the analytical interpretation and tangible guidance can be provided to those using handheld Raman spectroscopy in-field. To prove the concept, three NPSs were selected belonging to different classes and exhibiting different chemical scaffolds, namely, 5F-PB-22 (synthetic cannabinoid),<sup>[40,41]</sup> phenibut (GABA-A/B receptor agonist),<sup>[42]</sup> and N-Me-2-AI (aminoinda.ne).<sup>[43]</sup> In turn, a subset of four commonly used cutting agents and adulterants,<sup>[10,11,25,26,44]</sup> benzocaine, caffeine, creatine, and sodium glutamate was chosen, which will be referred to collectively as adulterants for the study.<sup>[10,11]</sup> The manuscript is laid out as follows: firstly, we carry out an initial evaluation of the spectral properties of all investigated NPS and adulterants; secondly, an in-depth analysis of our flipped detection approach is carried out using simulated street mixtures for each NPS; and lastly, we conclude by benchmarking our methodology to the Raman instrument's in-built algorithms. To the authors' knowledge, this work represents the first systematic study to investigate the role of adulterants and cutting agents as well as the effect on NPS concentration on the identification of NPS using handheld Raman spectroscopy.

### 3.1 | Initial evaluation and model development

Among other factors, a key challenge associated to the identification of NPS in street samples by portable spectroscopic techniques is often attributed to the large structural, and hence spectral, similarities between these substances and commonly used adulterants.<sup>[20,21,32]</sup> As a result, the development of novel in-the-field approaches

which are able to unequivocally discriminate between NPS and adulterants and further identify the psychoactive substance is of critical interest. Thus, the Raman spectra of three model systems were evaluated and then used to confirm the presence of the target analyte in the simulated street mixtures using our proposed flipped detection approach.

The feasibility of exploiting spectral differences between the NPS and adulterants was carried out by evaluating the raw Raman spectra followed by PCA model development. Figure 2 illustrates the Raman spectral profile of the three NPS and four adulterants selected as model compounds in this work. In line with their respective chemical structures (Figure 1) and their associated intrinsic scattering properties, the spectral profiles for 5F-PB-22 and to a lesser extent benzocaine, phenibut, and N-Me-2-AI are characterized by high-intensity Raman active bands. In turn, the decrease in conjugation in the case of creatine and particularly sodium glutamate results in weaker intensities and poorer S/N. It is of interest for the purpose of this work that the spectral profiles for the three NPS of interest exhibit intense Raman active bands which are unique to them and further differentiates them from the studied adulterants. Thus, this was a main focus of the spectral evaluation carried out in this study. The Raman spectrum of 5F-PB-22 exhibits a large number of strong and well-defined active bands. Among those we consider of particular note is the strong vibrational band as a result of the carbonyl stretching at  $ca\ 1712\text{ cm}^{-1}$ . While this vibrational band is also observed in the case of benzocaine and caffeine with significant intensity, their location at  $ca\ 1685$  and  $1699\text{ cm}^{-1}$ , respectively, and lower relative intensity makes us hypothesize that it can be used as a key spectral marker in the detection of 5F-

PB-22, and structural analogs, in complex mixtures. In conjunction with the latter, characteristic Raman active bands at  $ca\ 777$  and  $1531\text{ cm}^{-1}$ , associated to C-F vibration and pyrrole quadrant stretching mode, respectively, represent suitable vibrational markers due to their location and relative intensity. The vibrational mode for the C-F stretching motion could serve as a key marker for the detection of structural analogs exhibiting almost identical wavenumbers for this functional group, such as 5F-Apica ( $770\text{ cm}^{-1}$ ), 5F-Apinaca ( $774\text{ cm}^{-1}$ ), NM-2201 ( $770\text{ cm}^{-1}$ ) as well as AM-2201 ( $778\text{ cm}^{-1}$ ).<sup>[20]</sup> The spectral profile of phenibut is clearly dominated by a very strong active band located at  $ca\ 1000\text{ cm}^{-1}$ , associated to a 2, 4 and 6 radial in-phase stretching motion which is characteristic of monosubstituted benzenes. In addition, its Raman profile also features vibrational bands which can be ascribed to both semicircle and quadrant aromatic stretching modes located at  $ca\ 1410$  and  $1601\text{ cm}^{-1}$  respectively, also observed in the spectra of N-Me-2-AI and 5F-PB-22. Contrary to the case of phenibut, the spectral profile of N-Me-2-AI is characterized by a large number of moderate intensity vibrational bands. This progression is dominated by the signal associated to the in-plane C-H rocking vibrational motion at  $ca\ 1022\text{ cm}^{-1}$  as well as C-H wagging modes located at  $ca\ 777$  and  $847\text{ cm}^{-1}$ . It is of particular note that in the case of moderate Raman scatterers, the presence of more than one key spectral signature is often required for its unequivocal detection (vide infra).

Careful analysis of the Raman spectral profiles of the four adulterants reveals the complexity of developing a portable spectroscopic methodology for psychoactive substances, particularly in street samples which contain significant concentrations of benzocaine, a very strong Raman scatterer as well as caffeine and creatine. In turn, the complexities posed by sodium glutamate are different in nature and associated to the presence of a large number of low-intensity Raman active bands and poor S/N. This can result in large spectral correlations which are associated to high noise baseline levels and not key spectral signatures, potentially leading to false positives in samples characterized by large concentrations of this adulterant. The spectral profile of benzocaine features four strong Raman active bands at  $ca\ 864$ ,  $1279$ ,  $1606$ , and  $1683\text{ cm}^{-1}$ . The first two of these four bands can be ascribed to a C-H in-phase vibration mode of the conjugated core and a C-O stretching mode, respectively. The peak at  $1606\text{ cm}^{-1}$ , which dominates the spectral progression, can be associated to the quadrant vibration of the benzene moiety. We ascribe the lower wavenumber shift of the carbonyl vibrational band in benzocaine with respect to the observed value in 5F-PB-22 to the significant differences in the R groups of these aromatic esters

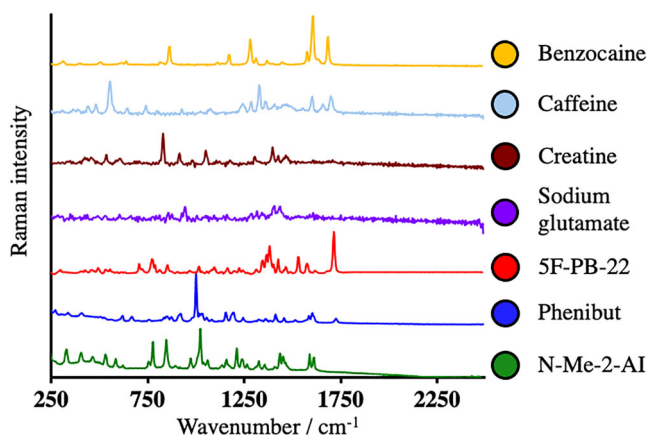


FIGURE 2 Experimental Raman spectral profiles of the different new psychoactive substance (NPS) and adulterants investigated in this work.  $\lambda_{\text{exc}} = 1064\text{ nm}$  [Colour figure can be viewed at [wileyonlinelibrary.com](http://wileyonlinelibrary.com)]

(Figure 1). Both caffeine and creatine are characterized by Raman spectra with the highest intensity bands below  $1000\text{ cm}^{-1}$ , associated to quadrant in-phase ( $555\text{ cm}^{-1}$ ) and C-O stretching motions ( $830\text{ cm}^{-1}$ ), respectively. The Raman profile of caffeine further features medium intensity bands at ca  $1330$  and  $1602\text{ cm}^{-1}$  which can be associated to semicircle and quadrant vibrational motions of the imidazole and pyrimidinedione moieties, respectively. In turn, bands located at  $916$  and  $1396\text{ cm}^{-1}$  in the spectrum of creatine are associated to an out-of-plane bending mode of the methylene group adjacent to the carbonyl and a C-N stretching motion, respectively. Lastly, the Raman spectrum of sodium glutamate exhibits a poor S/N, consistent with its aliphatic nature, with Raman active bands at  $1406$  and  $1435\text{ cm}^{-1}$  associated to O=O-CH<sub>2</sub> bending modes in both cases.

Subsequently, and to gain further insight into the spectral dissimilarities among these selected compounds, we subjected a dataset containing 10 replicates for each compound investigated to clustering methodologies using hierarchical complete linkage method and absolute correlation (Figure 3). We observed that despite the aforementioned spectral similarities, seven independent clusters were generated. This can be partially ascribed to the above-detailed key spectral markers. Importantly, each cluster was formed of 10 replicates, with all cluster representatives denoting replicates of the same standard material. We report larger relative distances between the cluster representatives (i.e. replicates) in the case of sodium glutamate, which can be readily attributed to the poor S/N observed in the Raman spectra of this adulterant. In turn, we report negligible relative distances among the cluster representatives in the case of benzocaine and 5F-PB-22, which we account for on the basis of their strong scattering properties. Interestingly, these results are consistent with three higher level clusters and two superclusters, one formed by the three NPS and the other one by the four adulterants. This suggests that there are key spectral differences that can be exploited to

differentiate the NPSs from the adulterants. Inspired by these outcomes, next, we subjected this dataset to PCA for an in-depth analysis of their spectral signatures. Three bespoke model systems, each containing one NPS and all four adulterants, were generated and subsequently evaluated in detail.

PCA models for each of the three subsets, each containing one NPS and all adulterants, were generated and subsequently analyzed. Given the large number of variables in the data matrix, first, we evaluated the effect of systematic data reduction without compromising their performance, denoted by amount of explained variance, particularly along the first three principal components which carry most of it. This is of significant interest in the development of algorithms, with the aim of reducing data processing times. We observed that, in line with previous studies on NPS,<sup>[20,23]</sup> the lack of spectral features in all cases beyond ca  $1750\text{ cm}^{-1}$  (Figure 2) allows for a significant reduction of the number of variables to be processed. This was confirmed by the analysis of the amount of explained variance in each developed model. In short, negligible changes in explained variance by the three first principal components were observed when narrowing the spectral region of interest to  $250\text{--}1750\text{ cm}^{-1}$  (46/20/18//42/21/19, 48/19/17//45/19/14, and 56/19/12//55/19/13% for full spectral range// $250\text{--}1750\text{ cm}^{-1}$  of 5F-PB-22, phenibut and N-Me-2-AI, respectively). It is noteworthy that in all cases, developed model systems were observed to account well for the total variance of the dataset, exhibiting explained variances  $>98\%$  for the first four principal components. It is also of importance that all chemometric models were generated employing raw spectral data to allow for further comparisons and benchmarking with instrument in-built algorithms. This highlights the robustness of these models which do not require preprocessing methodologies of the spectroscopic data. Figure 4 illustrates the developed model systems and their discriminative ability, where replicates for each substance cluster together and

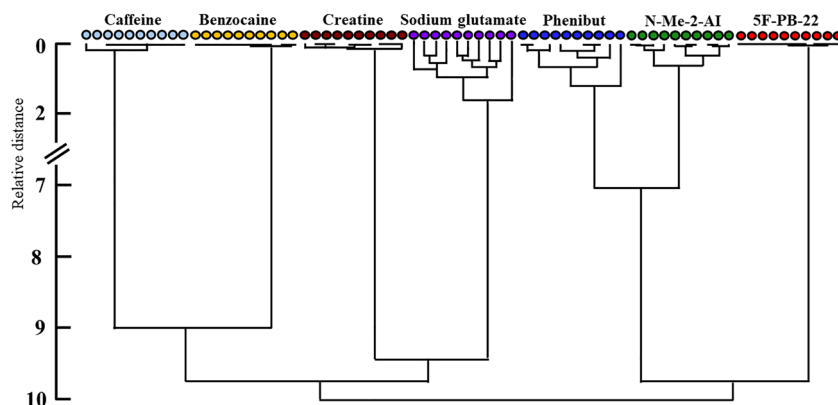


**FIGURE 3** Dendrogram illustrating the relationships between the Raman spectral profiles of all new psychoactive substance (NPS) and adulterants investigated in this work [Colour figure can be viewed at [wileyonlinelibrary.com](http://wileyonlinelibrary.com)]

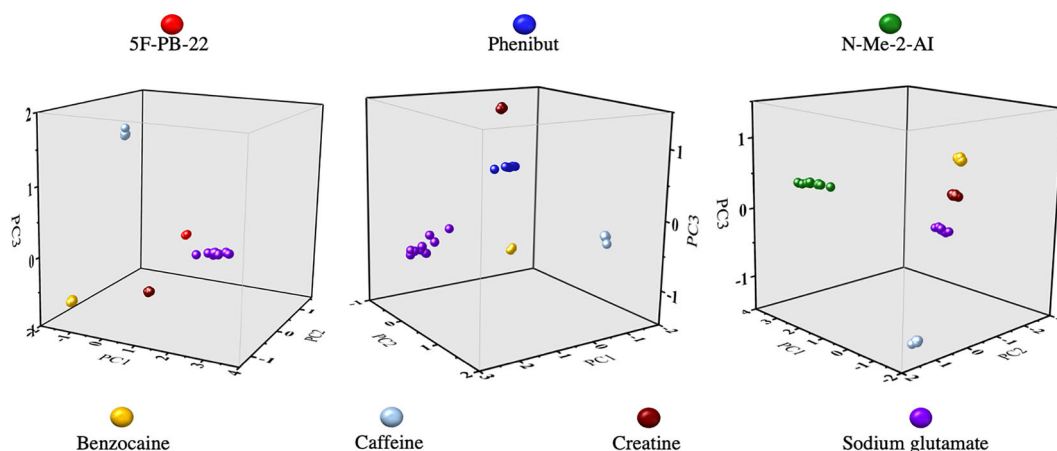


**FIGURE 4** Three-dimensional scores plots for each new psychoactive substance (NPS) and all adulterants generated using 10 replicates spectra per substance and 250–1750  $\text{cm}^{-1}$  spectral region [Colour figure can be viewed at [wileyonlinelibrary.com](https://onlinelibrary.wiley.com)]

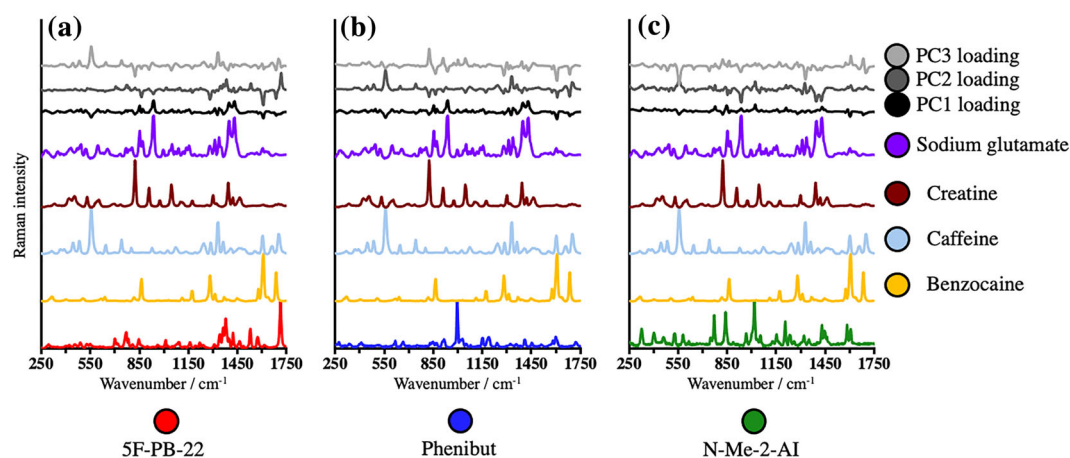


**FIGURE 5** Experimental Raman spectral profiles and line loadings for all three first principal components for each developed principal component analysis (PCA) model system [Colour figure can be viewed at [wileyonlinelibrary.com](https://onlinelibrary.wiley.com)]

occupy distinctly different regions in the three-dimensional scores plot with respect to other compounds in the subset. The latter, which is in line with observations made by hierarchical clustering analysis, can be judiciously associated to previously described Raman active chemical scaffolds and associated key spectral features. To further explore these observations, we went to examine in detail the line loadings for the three first principal components in each developed model system.

Careful evaluation of the three-dimensional scores plots in Figure 4 and associated spectral profiles and line loading plots in Figure 5 reveals that in agreement with hierarchical clustering analysis, replicates of sodium glutamate, phenibut, and to a lesser extent, N-Me-2-AI occupy larger regions of the three-dimensional scores plots when compared with their subset counterparts. It is of particular note that for all investigated cases, greater similarities in the three-dimensional score plots were

observed between the NPS and creatine as well as sodium glutamate and not benzocaine and caffeine, which exhibit greater relative intensities of the main Raman active bands (Figure 2). Nonetheless, clear delineation among all subset representatives in all three bespoke model systems is seen. In the case of the model system for 5F-PB-22, the observed lack of delineation between this NPS and creatine along the first principal component can be ascribed to similar spectral patterns in the region corresponding to semicircle stretching motions which is characterized by high intensity loadings in this principal component. In turn, the closely clustered together replicates of 5F-PB-22 exhibit successful delineation with respect to all other compounds along the second principal component. We associate the latter observation to the highest intensity loading for this component coinciding with the key spectral marker of 5F-PB-22 related to the carbonyl stretching at ca 1712  $\text{cm}^{-1}$  (Figure 5a).



Similarly, while replicates for phenibut are delineated along all first three principal components with respect to benzocaine, caffeine, and sodium glutamate, they exhibit a similar location in the three-dimensional scores plot when compared with creatine along the first principal component (Figure 4). The arguably poorer delineation with respect to scores of creatine can be attributed to C-N stretching Raman active bands of comparable intensity at ca  $1402\text{ cm}^{-1}$ . In turn, the observed delineation along the third principal component with respect to all other subset members can be attributed to phenibut's characteristic radial in-phase stretching motion which coincides with a medium intensity loading for this principal component and is absent in all other subset members. Interestingly, despite the absence of high-intensity Raman active bands in the spectrum of N-Me-2-AI, we observed a clear delineation along the first and, to a lesser extent, the second principal components among all subset representatives in the three-dimensional scores plot (Figure 4). The latter can be readily ascribed to spectral regions of high loadings in PC1 which coincide with key spectra markers, such as the C-H wagging motion at ca  $847\text{ cm}^{-1}$ , pyrimidinedione's quadrant vibrational motion at ca  $1606\text{ cm}^{-1}$ , quadrant in-phase vibration at ca  $556\text{ cm}^{-1}$  as well as the C-O stretching at ca  $824\text{ cm}^{-1}$ , which are characteristic of N-Me-2-AI, benzocaine, caffeine, and creatine, respectively.

Our bespoke model systems reveal that successful detection of target NPS in complex street mixtures using traditional approaches can be compromised not only by known strong Raman scatterer materials but also by weaker ones, such as creatine and sodium glutamate. This observation can be employed to explain, at least partially, the failure of previous efforts exploiting detection protocols consisting in maximizing the spectral similarities of NPS-containing mixtures (i.e., lower purity) to those of reference standard materials (i.e., high purity).<sup>[24,25,28,45]</sup> In cases where chemometric techniques were employed, such as PCA, detection was largely based on visual inspection of three-dimensional scores plots and the “distance” between sample scores and those of reference standard materials for known NPS.<sup>[20,23,29,31,46,47]</sup> However, such approaches are not appropriate for the analysis of complex mixtures where the spectral profile of the sample is dominated by additives rather than the target analytes. In response to these observations, in this work, we detail below an innovative flipped detection approach based on coupling Raman spectroscopy and chemometrics for the unambiguous detection of these relevant analytes in complex mixtures. Contrary to previous methodologies, we propose a critical change whereby the identification of the target NPS in the mixture is associated to differences with respect to the adulterants rather

than similarities with respect to the continuously growing dataset of NPS standards. We based our approach on a two-step methodology which can be easily implemented as an in-built algorithm in portable Raman spectrometers. In Step 1, contrary to previous efforts, we attribute the presence of the NPS to dissimilarities with respect to adulterants rather than similarities when compared with NPS reference standard materials. This is done by projection analysis of the complex mixtures' spectra on generated PCA models, with such dissimilarities being consistent with delineation of scores of the mixtures with respect to these of reference standards of the adulterants. Subsequently, Step 2, which works alongside Step 1, is used to unequivocally confirm the detection of the NPS by means of key spectral signatures which are unique to target NPS/NPS classes to which the target analyte belongs. In other words, if the delineation observed in Step 1 is caused by a non-NPS, this would not be confirmed in Step 2 due to the lack of key spectral signatures. In the following sections, we carry out an in-depth evaluation of our proposed methodology by means of the projection of spectra from samples of known composition used to mimic the complexity of street drugs, always containing one NPS and up to four adulterants, in the generated bespoke model systems. These so-called TS were generated using a DoE methodology in order to account for the plethora of possible sample compositions, resulting in 21 TS for each NPS. The number of components as well as their concentration in the generated TS was systematically increased and decreased, respectively, for added complexity. As such, the concentration of the NPS in our test dataset ranged from 62.6% w/w to 16.0% w/w quinary mixtures, including 6.6% w/w binary and ternary mixtures.

## 3.2 | Detection of NPS in mixtures using the flipped approach

### 3.2.1 | Binary mixtures

Firstly, we evaluated the ability of our proposed flipped methodology in the detection of the NPS in binary mixtures containing 6.6 (TS 2–5) and 53.3% w/w (TS 6–9) concentrations of these target analytes (Table 1). Again, TS results were projected onto the PCA model systems and will be discussed in terms of Step 1 and 2 (as mentioned above), where Step 1 denotes the flipped methodology in relation to previous approaches and Step 2 represents the confirmation underpinned by key spectral signatures which are unique to the target analyte. In the following, a successful performance of the proposed methodology is considered when the presence of the NPS

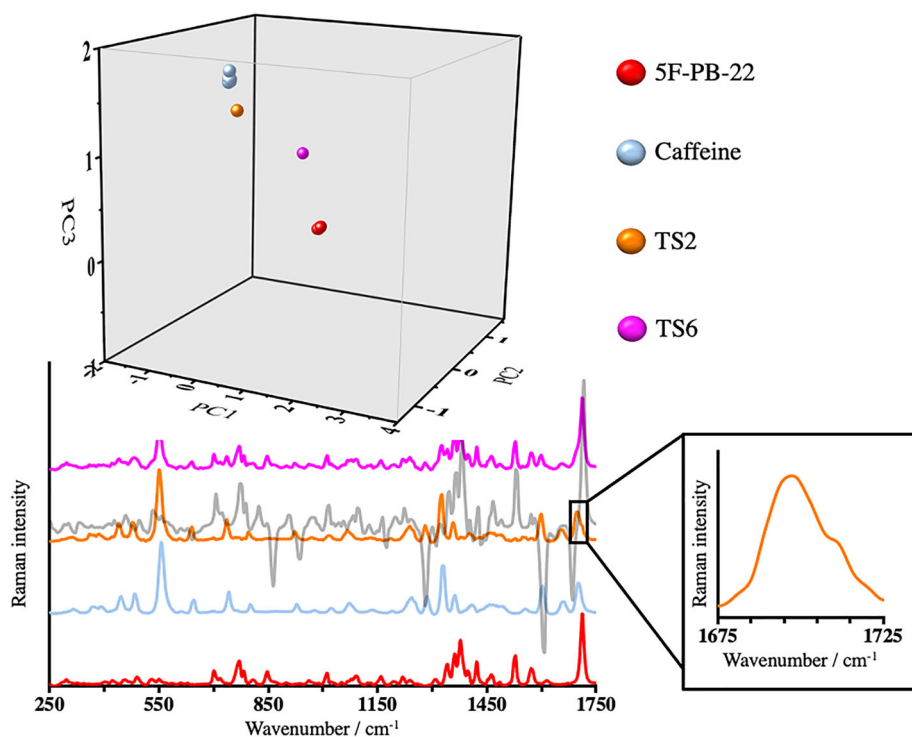


**FIGURE 6** Three-dimensional scores plot (top) for 5F-PB-22 model system, showing selected scores for 5F-PB-22 and caffeine standards ( $n = 10$ ) and projections for TS2 and TS6 (average,  $n = 4$ ). Relevant Raman spectral profiles and line loading for PC2 (bottom—inset illustrates key spectral signature of TS2) [Colour figure can be viewed at [wileyonlinelibrary.com](http://wileyonlinelibrary.com)]

is anticipated by dissimilarities observed in Step 1 and further confirmed based on spectral signatures in Step 2. For example, for 5F-PB-22 containing binary mixtures with 53.5% w/w concentrations, we report delineation with respect to all adulterants along the second principal component (Step 1) which can be attributed to the Raman active band of this NPS at ca  $1712\text{ cm}^{-1}$  and the high intensity loading at this wavenumber in PC2 (Step 2) (Figure SI.3.5–8). This example would be considered as a successful performance of the proposed flipped methodology. Along these lines, we anticipate this observation to facilitate the detection of existing structural analogs to 5F-PB-22, namely, PB-22 and FDU-PB-22, which are characterized by similar vibrational frequencies for the carbonyl stretching motion at  $1708$  and  $1717\text{ cm}^{-1}$ , respectively.<sup>[20]</sup> In addition, these compounds also exhibit Raman active vibrational bands associated to the quadrant stretching motion in the pyrrole moiety which closely coincide with that observed for 5F-PB-22 ( $1531$  and  $1535\text{ cm}^{-1}$  for PB-22 and FDU-PB-22, respectively).<sup>[20]</sup> Despite the delineation with respect to the scores for caffeine, identification of the NPS spectral signatures in the Raman spectrum of TS6 requires a more detailed analysis when compared with TS containing other adulterants. We ascribed this observation to caffeine's carbonyl Raman active band which closely coincides with that of 5F-PB-22. As a result, we anticipated the detection of this NPS in TS2 to represent a challenge, due to the significantly lower concentration of 5F-PB-22. In fact, the spectral signature of this NPS in the Raman

spectrum of the sample is denoted by an inflection in the higher intensity contribution from caffeine at ca  $1707\text{ cm}^{-1}$ . Nonetheless, the delineation with respect to caffeine's scores is demonstrated (Figure 6). Identification in analogous TS containing creatine and sodium glutamate is less complex due to the weaker relative intensity of these adulterants when compared with benzocaine and caffeine (Figure SI.3.3–4). In the case of TS3, the presence of the target analyte in the analyzed mixture based on the dissimilarity with respect to adulterants is readily confirmed in the second step of our methodology due to the lack of spectral overlap between key Raman active bands of benzocaine and 5F-PB-22.

Initial inspection of the line loadings for the model system for phenibut (Figure 4) could anticipate its detection in TS6–9 mixtures to be hindered due to the key spectral feature of this substance being represented solely by a medium intensity loading in the third principal component (Figure 5b). Interestingly, we report successful performance of our novel methodology for these phenibut-containing binary mixtures (Figure SI.3.25–28), albeit smaller relative displacements are observed in the three-dimensional scores plot when compared with the previously described NPS, 5F-PB-22. As a result, the evaluation of lower concentration TS, TS2–5, is of particular interest. It is of note that while closer location of the sample scores with respect to the NPS was observed for 53.3% w/w binary samples containing creatine and phenibut (Figure SI.3.27), the opposite is observed when the concentration is lowered to 6.6% w/w (Figure SI.3.23). We

attribute these findings to the above-mentioned lower relative intensity and larger noise levels in the Raman spectrum for these adulterants, which linked to the low-intensity key spectral signatures at this NPS concentration, results in signals which are only slightly above the noise level. In turn, the flatter baseline characteristic of benzocaine and caffeine contributes towards discriminating those phenibut-induced inflections (Figure SI.3.21–22). Identification of N-Me-2-AI in 53.3% w/w binary mixtures (Figure SI.3.45–48) is facilitated by high intensity loadings along the first principal component at ca 777 and 1022  $\text{cm}^{-1}$  which coincide with C-H wagging and rocking vibrational motions of this substance, respectively (Figure 5c). Due to the different intensity nature of these loadings, the previously described finding for phenibut does not apply to this NPS. The intrinsic weaker scattering behavior of this aminoindane is counteracted by the presence of the two high intensity loadings which aids in its detection in complex mixtures. In fact, when compared with 6.6% w/w TS containing 5F-PB-22, the intensity of the NPS spectral signatures in the Raman spectrum of TS containing benzocaine and caffeine is arguably lower. However, appropriate chemometric-aided identification is facilitated due to the synergistic contribution of the two loading bands as illustrated in Figure 7.

In all binary mixtures investigated, and irrespective of the adulterant present in the mixture, we report successful performance of our flipped approach, meaning that delineation in the scores plots is consistent with key spectral signatures of the target analyte, even in the case of TS 2–5, which importantly denote the lowest concentration of NPS to be detected in solid-state samples to date

by portable methodologies. Next, the complexity of the simulated street samples was increased by adding a second adulterant and maintaining the low concentration of the NPS, at 6.6% w/w.

### 3.2.2 | Ternary mixtures

Subsequently, we explored in detail mixtures containing NPS at 6.6% w/w and two adulterants (TS10–15) at equal (46.6% w/w) concentrations. These were compared with TS2–5 to evaluate the role of a second adulterant in the detection capabilities of the bespoke model systems while maintaining equal concentration of the target analyte. In the case of ternary TS containing the synthetic cannabinoid 5F-PB-22, similar to the observations made for binary mixtures, the presence of the target analyte was detected in all cases during Step 1 of the process, exemplified by clear delineation in the respective score plots. Detection of the target analyte in TS containing creatine and sodium glutamate was confirmed in Step 2 and can be readily attributed to the adulterants lack of high-intensity carbonyl active bands and their overall weaker scattering properties (Figure SI.3.9–14). Along those lines, it was of particular interest the evaluation of TS10 which contained benzocaine and caffeine, in light of the presence of high intensity bands associated to carbonyl stretching motions in both adulterants (*vide supra*). In Step 2, careful evaluation of the Raman spectrum for TS10 reveals a complex convoluted Raman active band with a maximum at ca 1685  $\text{cm}^{-1}$ , hence, dominated by the carbonyl stretching band of benzocaine, which is further in line with its concentration and greater scattering

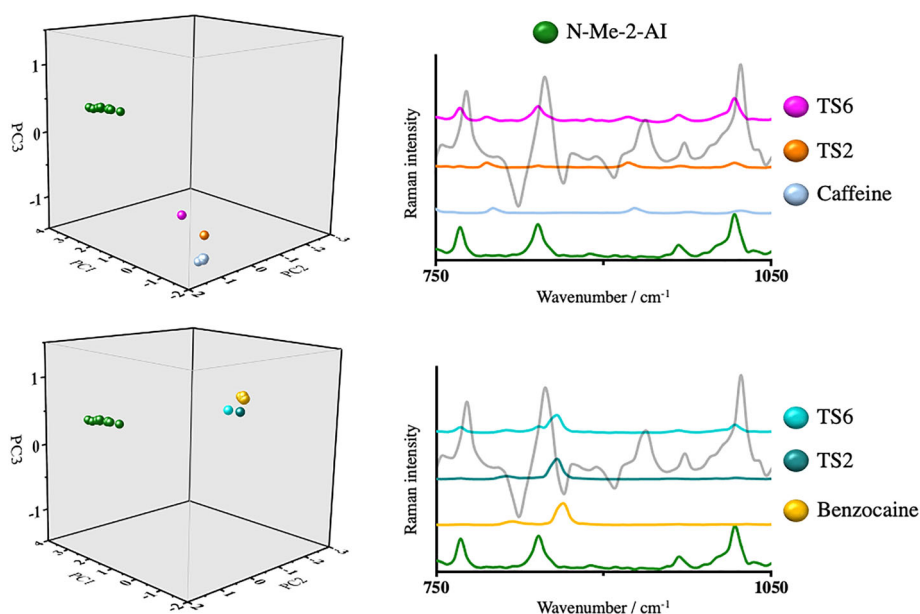


**FIGURE 7** Three-dimensional scores plot (left) for N-Me-2-AI model system, showing selected scores for benzocaine (bottom) and caffeine (top) standards ( $n = 10$ ) as well as projections for binary mixtures (average,  $n = 4$ ). Associated Raman spectral profiles and line loading for PC1 (right) [Colour figure can be viewed at [wileyonlinelibrary.com](http://wileyonlinelibrary.com)]

properties when compared with caffeine standard. The convoluted Raman active band features two clear inflections with centers located at ca 1699 and 1712  $\text{cm}^{-1}$ , which are characteristic of the carbonyl stretching Raman active bands of caffeine and 5F-PB-22, respectively (Figure 8), thus enabling detection of the NPS in this mixture using a signature Raman band. This observation reinforces the successful performance of the developed methodologies, even for samples with low concentrations of the target analytes.

Target analyte detection in ternary, phenibut-containing mixtures is attributed to phenibut's key spectral marker at ca 1000  $\text{cm}^{-1}$ . Despite the larger relative intensity of the spectra of benzocaine and caffeine, the lack of Raman active bands of significant intensity in this spectral region facilitates the detection of this NPS. In turn, the weak active band in the spectrum of sodium glutamate at ca 1006  $\text{cm}^{-1}$  (Figure 2) was anticipated to constitute an added complication. However, careful evaluation of the three-dimensional scores plot (Step 1) and Raman spectra (Step 2) confirms isolation of the NPS key spectral feature in the spectrum of TS12 as well as TS14–15 from the adulterants (Figure SI.3.31, 33–34, respectively). Evaluation of the performance of the model system in the detection of N-Me-2-AI in these ternary mixtures further highlights the previously described importance of the close alignment between two Raman active bands in the spectrum of this NPS at ca 777 and 1022  $\text{cm}^{-1}$  with high intensity loadings along the first

principal component. In the case of TS10, detection of the target analyte is facilitated by the bimodal feature of the aminoindane (Figure SI.3.49). In short, the presence of a caffeine-related weak active band at ca 1033  $\text{cm}^{-1}$  increases the complexity of unequivocally ascribing the spectral feature of the spectrum of TS10 to N-Me-2-AI solely on the basis of the peak at ca 1022  $\text{cm}^{-1}$ . However, the successful detection of the NPS in this complex mixture is facilitated by the flipped approach: Step 1 is consistent with the clear displacement of the score of TS10 with respect to the scores of both adulterants, and Step 2 indicates the appearance of a measurable signal in the spectrum of TS10 at ca 777  $\text{cm}^{-1}$ , associated to the C-H wagging motion in N-Me-2-AI (Figure 9). We further investigated whether the signal at 1022  $\text{cm}^{-1}$  can be attributed to caffeine by evaluation of TS11, which contains creatine instead of benzocaine. Due to the weaker scattering properties of creatine, the relative intensity of caffeine and N-Me-2-AI spectral features in the spectrum of the TS increased. Given that the concentration of both components remains constant, we can attribute the higher relative intensity of the band at 1022  $\text{cm}^{-1}$  to the NPS, as illustrated in Figure 9. In addition, we anticipate the observations in Step 2 of the process to be able to facilitate the detection of other structurally related aminoindanes, such as 2-AI, which is characterized by remarkably similar key active Raman bands at 778/857 and 1024  $\text{cm}^{-1}$  for C-H wagging and rocking motions, respectively.<sup>[20]</sup>

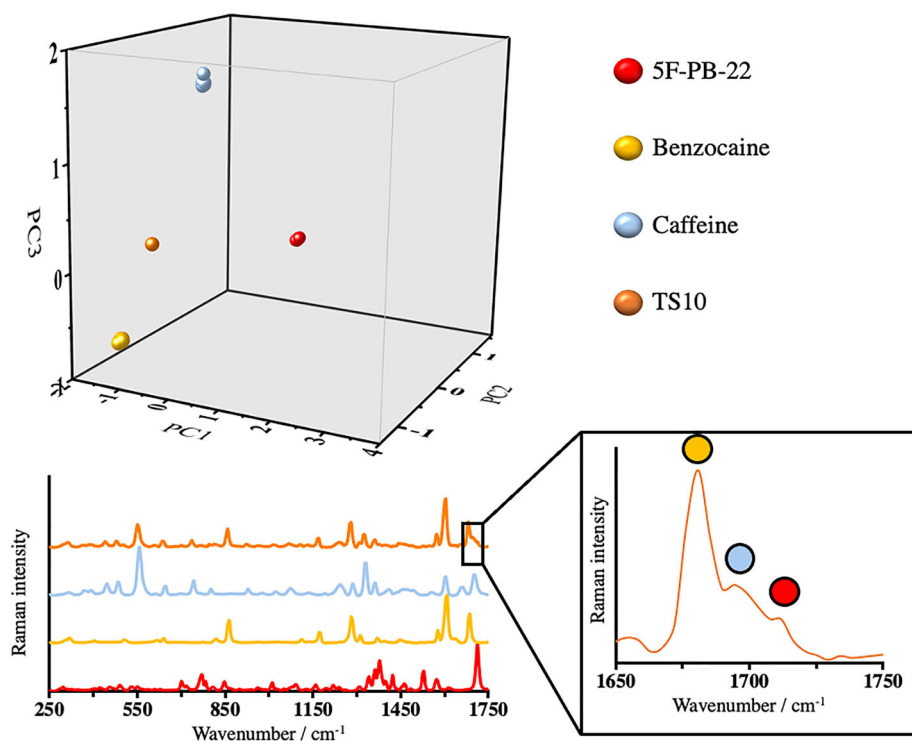


**FIGURE 8** Three-dimensional scores plot (top) for 5F-PB-22 model system, showing selected scores for benzocaine and caffeine standards ( $n = 10$ ) as well as TS10 ternary mixture (average,  $n = 4$ ). Associated Raman spectral profiles (bottom—inset illustrates in detail the described convoluted Raman active band in the spectrum of TS10) [Colour figure can be viewed at [wileyonlinelibrary.com](http://wileyonlinelibrary.com)]

### 3.2.3 | Quinary mixtures

To add a further layer of complexity, we devote this next part of the manuscript to testing the flipped detection of NPS in quinary mixtures where the concentration of the target analyte ranges from 62.6 to 16% w/w and the adulterants exhibit variable concentrations (TS16–21). Despite all four adulterants being present in TS16, clear dissimilarities with respect to adulterants were observed in all cases, which can be attributed to the high concentration of the NPS (Figures SI.3.20, SI.3.40 and SI.3.60 for 5P-PB-22, phenibut, and N-Me-2-AI containing mixtures) and hence easily identified key vibrational bands as described above for binary and ternary mixtures. On progression to TS21, the concentration of the target analyte is significantly decreased from 62.6% to 25.3% w/w and the concentration of the adulterants increased from 9.3% to 18.6% w/w in all cases. While the relative concentration of the NPS with respect to each individual adulterant is larger than for other investigated TS (e.g., TS6–9), the synergistic effect of spectral features of all adulterants could compromise successful NPS detection. For all three target NPS, the flipped approach resulted in successful detection of the NPS in TS21 by means of significant displacements of the score for TS21 from the scores of the

adulterants (Step 1) and confirmed detection by means of key vibronic bands in TS which coincide with key loadings (Step 2). Figure 10 illustrates these findings in the case of N-Me-2-AI, which is arguably the most complex of all three TS21 quinary mixtures and its comparison with TS16. In both cases, we demonstrate for Step 1 clear delineation of the scores plots for these TS with respect to those of adulterants and for Step 2 key spectral features at 777 and 1022  $\text{cm}^{-1}$ . It is of note that similarly to the case described for TS10 and TS11 (Figure 9), the vibrational band of N-Me-2-AI centered at ca 777  $\text{cm}^{-1}$  is critical in confirming the detection of the analyte, particularly when the mixture presents caffeine as an adulterant. While the intensity of these two key bands in the Raman spectrum of TS21 is lower than that observed in the spectrum of TS16, careful evaluation ensures the unambiguous presence of the NPS in the mixture, as illustrated in Figure 10.

Next, quinary TS containing 16.0% w/w of the NPS and 56.0% w/w of one of the adulterants in the mixture were analyzed. Despite large (56.0% w/w) concentrations of creatine and sodium glutamate in TS19–20 quinary mixtures of 5F-PB-22, the flipped approach led to clear delineations in the three-dimensional scores plots associated to the key spectral signatures (Figure SI.3.18–19).

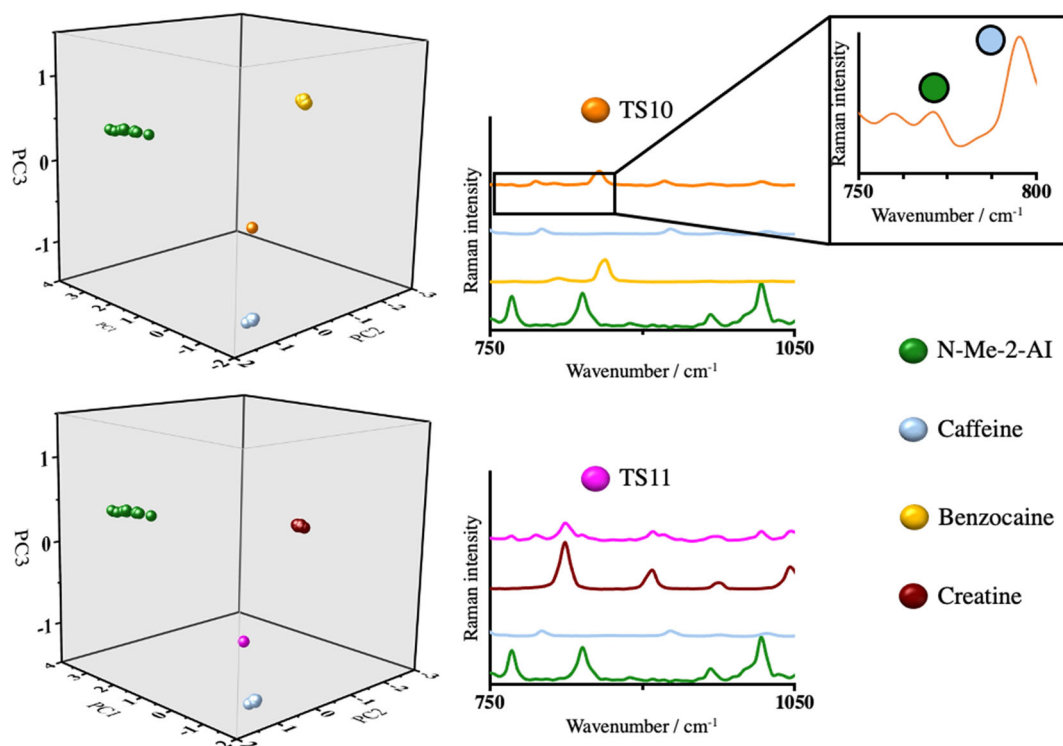


**FIGURE 9** Three-dimensional scores plot (left) for N-Me-2-AI model system, showing selected scores for benzocaine, caffeine and creatine standards ( $n = 10$ ) as well as scores for TS10 (top) and TS11 (bottom) ternary mixture projections (average,  $n = 4$ ). Associated Raman spectral profiles (right—inset illustrates in detail the described convoluted Raman active band in the spectrum of TS10) [Colour figure can be viewed at [wileyonlinelibrary.com](http://wileyonlinelibrary.com)]

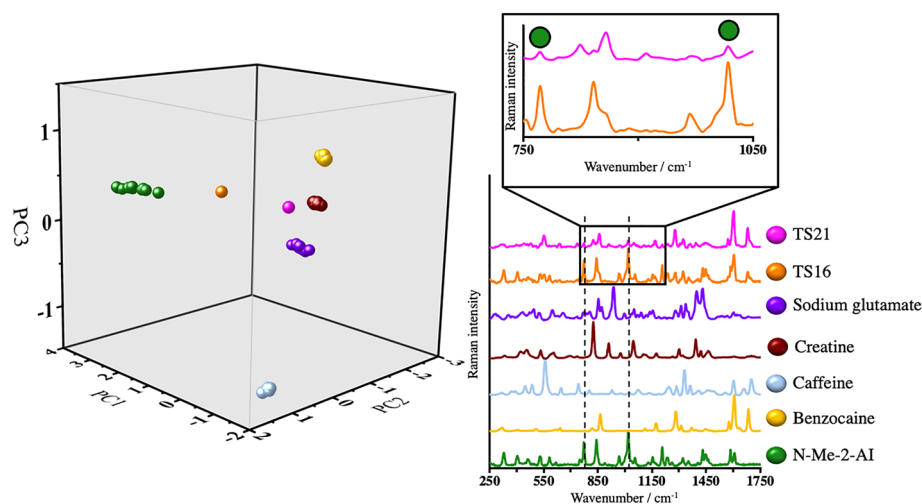


**FIGURE 10** Three-dimensional scores plot (left) for N-Me-2-AI model system, showing selected scores for all adulterants ( $n = 10$ ) as well as scores for TS16 and TS21 quinary mixture projections (average,  $n = 4$ ). Associated Raman spectral profiles (right—inset illustrates key features for TS16 and TS21 in the spectral region of interest, 750–1050  $\text{cm}^{-1}$ ) [Colour figure can be viewed at [wileyonlinelibrary.com](http://wileyonlinelibrary.com)]

The presence of high concentrations of benzocaine was observed to have a lower impact when compared with caffeine-containing TS, despite the stronger scattering properties of the former. In fact, the spectral signatures of the Raman spectrum for TS17 at ca 1690  $\text{cm}^{-1}$  are characterized by two inflections in a vibronic complex dominated by the carbonyl stretching signal from 5F-PB-22 (Figure SI.3.16). Similar trends were observed for phenibut containing mixtures (Figure SI.3.36–39). However, the ease of detection of this NPS in quinary mixtures containing benzocaine and caffeine as the major constituents was reversed with respect to samples containing 5F-PB-22, which we ascribed to the lack of caffeine-related vibrational bands at ca 1000  $\text{cm}^{-1}$  and the greater scattering intensity of benzocaine. In line with observations previously described for TS containing N-Me-2-AI, the bimodal nature of the key spectral signatures is critical for its detection. The latter is of particular note in the case of TS18 (Figure SI.3.57), which contains 56.0% w/w of benzocaine, given the significant differences in relative intensity with respect to this aminoindane. Despite this high adulterant concentration, we report successful performance of our approach with clear delineation of the score plot for TS18 with respect to those of benzocaine in the three-dimensional scores plot (Step 1), consistent with the low intensity bands in the Raman spectrum of this TS at ca 777 and 1022  $\text{cm}^{-1}$  associated to the presence of N-Me-2-AI (Step 2).

### 3.3 | Performance of instrument in-built algorithms

Lastly, in order to systematically evaluate the performance of the instrument's in-built algorithms and to further validate our developed methodology, we benchmark

our detection results with those yielded by in-built algorithms in our portable Raman spectrometer of choice (Table SI.4.1–4), including both single- and multiple-component output algorithms. It should be noted that (i) in all cases, the same Raman spectra as those used for the flipped methodology were used for the instrument in-built algorithms and (ii) again, successful performance of the flipped approach was considered when the delineation of the mixture's score with respect scores of adulterants (Step 1) can be further confirmed with key spectral Raman active bands, in line with model loadings (Step 2). We report a striking improvement over the performance exhibited by commercially available algorithms which further warrants the development of novel approaches as the one reported herein.

The in-built Wavelet algorithm is a single-component output algorithm, which makes it an attractive choice based on its simplicity for the nonqualified end user and facilitates rapid decisions when compared with more complex multiple-component output algorithms. In light of the spectral similarities between adulterants and NPS, it was deemed as critical to first determine the correlation results of the neat adulterants to each NPS of interest in order to establish criteria for false positives before further interpretation. To do this, three bespoke libraries, each containing one NPS, and the four adulterants were created, and the correlations were determined. In all cases, samples evaluated contained 150 mg of the relevant adulterant standard and were analyzed a total of four times. In line with the detailed spectral interpretation, we report larger correlation results for sodium glutamate to all investigated NPS. Irrespective of the adulterant, larger correlations were observed to phenibut and N-Me-2-AI, which are in agreement with their poorer Raman scattering properties when compared with the synthetic cannabinoid, 5F-PB-22. Based on these results summarized in

Table 2, it is suggested that values below 0.25 must be interpreted with care and as plausible false positives when evaluating the results.

On evaluating the performance of the in-built single-component output algorithm, consistent (i.e., 4/4) positive correlations across all NPS were only observed in the case of binary mixtures containing large (53.3% w/w) concentrations of creatine (TS8) and sodium glutamate (TS9), which can be further ascribed to the poor Raman scattering properties of these adulterants (Figure 2). Positive correlations were also observed for TS16, which can be associated to the large concentration (62.6% w/w) of the NPS in this sample and despite the presence of all four adulterants. Low and/or inconsistent correlations were observed for TS containing low concentrations of the NPS and strong scattering adulterants such as benzocaine and caffeine. We consider of particular note the lack of correlation and thus successful detection in the case of quinary mixture, TS21, which contains an arguably large concentration of the NPS (25.3% w/w), yet identification of key spectral makers for the NPS was facilitated using the flipped approach. Along these lines, we observed in all cases correlations in ternary samples (TS10–15) to be below the above stated threshold for false positives. While this can be attributed to the increased sample complexity with respect to binary mixtures as well as the low NPS content (6.6% w/w), the flipped methodology successfully accounted for the NPS present in these simulated street mixtures. These highlights for complex NPS mixtures, evaluating these Raman spectra using a flipped approach, can facilitate improved detection of NPS, via key spectral markers, over traditional approaches and also with respect to in-built algorithms.

Next, we evaluated the correlation results employing a multiple-component output algorithm in-built in the portable Raman spectrometer and compared these to our reported approach. Due to the complexity of the TS investigated in this study, it was of interest to evaluate a multiple-component output algorithm, that is, capable of correlating the unknown spectrum to one or more reference spectra within the chosen library. It should be noted

that although this type algorithm denotes a superior system for the evaluation of complex mixtures, the generated outputs also require greater expertise from the end user. It is of note the unsuccessful performance for binary mixtures containing 6.6% w/w of the NPS in all cases bar TS containing 5F-PB-22 and sodium glutamate. This can be associated to the intrinsic Raman scattering properties of both compounds and further represents a significant improvement over the single-component algorithm. Interestingly, while successful detection of the target analyte was achieved in all cases for higher concentration binary mixtures (TS6–9), in some cases such as phenibut and N-Me-2-AI containing samples, higher correlations were observed for adulterants and not the NPS. This significantly increases the complexity for the end user and could potentially lead to false positives if the correlation contribution is predominantly from the adulterant. In the case of ternary mixtures, performance of this in-built algorithm was observed to be poor and successful detection was only possible for some replicates of TS containing creatine and sodium glutamate as adulterants (Table SI.4.2–4). While this could be accounted for based on the NPS concentration in these mixtures (6.6% w/w), it also highlights the capabilities demonstrated by our flipped methodology, able to unequivocally detect the target NPS in all evaluated ternary mixtures. Lastly, the scenario in the case of quinary mixtures varies significantly based on the concentration of the NPS, with consistently appropriate correlations only observed for TS16, which can be attributed to the high (62.6% w/w) NPS concentration. This represents an improvement over the performance observed for these TS with the single-output algorithm. In turn, we report inconsistent correlations for all TS17–21, irrespective of the target NPS. For these types of samples specifically, the flipped detection provides an alternative approach to focus on key spectral signatures when in the presence of common adulterants. Figure 10 nicely illustrated the successful performance afforded by our novel method for TS21 containing N-Me-2-AI. It is of note that the results for this TS employing the multiple-component output are

**TABLE 2** Correlation results for adulterants to NPS using bespoke libraries and the in-built wavelet algorithm

Adulterant	Correlation		
	5F-PB-22	Phenibut	N-Me-2-AI
Benzocaine	0.04 ± 0.01	0.11 ± 0.01	0.19 ± 0.01
Caffeine	0.04 ± 0.02	0.12 ± 0.01	0.10 ± 0.01
Creatine	0.02 ± 0.01	0.09 ± 0.02	0.02 ± 0.01
Sodium glutamate	0.16 ± 0.03	0.23 ± 0.03	0.19 ± 0.03

*Note:* Results expressed as average and uncertainties as one standard deviation from 4/4 reported correlations.

Abbreviation: NPS, new psychoactive substance.

inconclusive, with the target NPS only being reported for one out of four replicates.

## 4 | CONCLUSIONS

In conclusion, we report a novel and elegant approach for the successful utilization of portable Raman technologies for the unequivocal detection of NPS in complex mixtures, such as those encountered by law enforcement officers in the field. It has been previously shown that so-called traditional approaches whereby the identification of the target analyte is ascribed to spectral similarities to reference standard materials in available libraries are inappropriate in cases where the target analyte is in low concentrations in combination with adulterants. To bypass these shortcomings, herein we proposed a flipped two-step approach which associates the presence of the NPS on the spectral dissimilarities with respect to adulterants (Step 1) rather than similarities to known NPS and then further facilitates unequivocal NPS detection by means of key spectral signatures in their Raman profile (Step 2). To prove this concept, three NPSs of interest were selected, 5F-PB-22, phenibut, and N-Me-2-AI which possess distinctly different chemical scaffolds, hence belonging to different NPS classes. Additionally, four widely used adulterants were chosen as the mixture matrix, namely, benzocaine, caffeine, creatine, and sodium glutamate. To account for the plethora of possible samples containing these compounds, we generated a subset of TS by a DoE-guided approach. These resulted in 21 binary to quinary simulated street samples, with NPS concentrations ranging from 6.0% to 62.6% w/w. We observed our proposed methodology to be able to detect the target analyte, even in cases where the NPS concentration was as low as 6.0% w/w, representing the lowest concentration detected in the solid-state by portable Raman methodologies to date. In those TS posing extra identification complexity, we observed that the unequivocal detection of 5F-PB-22 and phenibut containing mixtures was particularly afforded by key Raman active bands, such as those associated to carbonyl and radial in-phase stretching modes located at ca 1712 and 1000  $\text{cm}^{-1}$ , respectively. In the case of N-Me-2-AI, detection is observed to be facilitated by a bimodal feature from vibrational modes ascribed to C-H wagging and rocking motions at 777 and 1022  $\text{cm}^{-1}$ . Importantly, we went on to benchmark these results with those yielded by single- and multiple-component output in-built algorithms. Irrespective of the output mode of the in-built algorithm, unsuccessful and/or inconsistent performance was observed for all simulated samples with NPS concentration  $\leq 53.3\text{w/w}\%$ , particularly in ternary and quinary mixtures. In comparison, the flipped

method facilitated the detection of the NPS in these mixtures in all cases, thus uniquely exploiting the spectral dissimilarities between NPS and their common adulterants to enabled detection of the NPS via key spectral markers. As a result, we anticipate this work to be a critical change in the detection of NPS and to further denote a blueprint for the realization of novel approaches for the detection of target analytes in complex mixtures.

## ACKNOWLEDGEMENTS

We acknowledge the European Commission for funding under the Drug Prevention and Information Programme 2014-16, contract number JUST/2013/DPIP/AG/4823, EU-MADNESS project and JUST/ISEC/DRUGS/AG/6428, EPSNPS project. JC-C acknowledges funding for AAA from the Analytical Chemistry Trust Fund (ACSS 17/025) and the University of Hertfordshire under the Proof-of-Concept funding scheme. Open access funding enabled and organized by Projekt DEAL.

## CONFLICT OF INTEREST

The authors declare no competing financial interest.


## AUTHOR CONTRIBUTIONS

**Jesus Calvo-Castro:** conceptualization, methodology, validation, formal analysis, writing – original draft, visualization, supervision, project administration, and funding acquisition. **Steve N. Tchakounte:** investigation and data curation. **Valentina Guarino:** validation, formal analysis, investigation, and data curation. **Adeel A. Ahmed:** data curation. **Jacqueline L. Stair:** methodology, resources, writing – original draft, supervision, project administration, and funding acquisition.

## DATA AVAILABILITY STATEMENT

The data that support the findings of this study are available from the corresponding author upon reasonable request.

## ORCID

Jesus Calvo-Castro  <https://orcid.org/0000-0003-1031-8648>

Adeel A. Ahmed  <https://orcid.org/0000-0002-7013-7710>

## REFERENCES

- [1] D. K. Tracy, D. M. Wood, D. Baumeister, *BMJ (Online)*. <https://doi.org/10.1136/bmj.i6848>
- [2] United Nations on Drugs and Crime. (UNODC), Current NPS threats, Vol. 3, 2020.
- [3] Public Health England, A review of new psychoactive substances in mental health settings, 2017.
- [4] P. I. Dargan, D. M. Wood, *Novel Psychoactive Substances: Classification, Pharmacology and Toxicology* 2013.



- [5] H. Regunath, V. K. Ariyamuthu, P. Dalal, M. Misra, *Hemodialysis International* **2012**, *16*, S47.
- [6] C. Wells, *Health Statistics Quarterly* **2009**, *43*, 48.
- [7] Parliament, UK, Psychoactive Substances Act **2016**.
- [8] M. Rychert, C. Wilkins, *Drug Test. Anal.* **2016**, *8*, 768.
- [9] M. P. Elie, L. E. Elie, M. G. Baron, *Drug Test. Anal.* **2013**, *5*, 281.
- [10] C. Cole, L. Jones, J. McVeigh, A. Kicman, Q. Syed, M. A Bellis, Center for Public Health, Faculty Of Health And Applied Sciences, Liverpool **2010**, 1.
- [11] C. Cole, L. Jones, J. McVeigh, A. Kicman, Q. Syed, M. Bellis, *Drug Test. Anal.* **2011**, *3*, 89.
- [12] J. P. Smith, O. B. Sutcliffe, C. E. Banks, *Analyst* **2015**, *140*, 4932.
- [13] P. M. Geyer, M. C. Hulme, J. P. B. Irving, P. D. Thompson, R. N. Ashton, R. J. Lee, L. Johnson, J. Marron, C. E. Banks, O. B. Sutcliffe, *Anal. Bioanal. Chem.* **2016**, *408*, 8467.
- [14] European Commission, Customs 2020 REPORT CLEN Project Group on Designer Drugs and Other Illicit Products, 3rd meeting, **2020**.
- [15] European Monitoring Centre for Drugs and Drug Addiction. (EMCDDA), Drug checking as a harm reduction tool for recreational drug users: opportunities and challenges, **2017**.
- [16] A. O'Hagan, R. Hardwick, *Forensic Res. Criminol. Int. J.* **2017**, *1*.
- [17] J. L. Vicente, H. Chassaing, M. V. Holland, F. Reniero, K. Kolář, S. Tirendi, I. Vandecasteele, I. Vinckier, C. Guillou, *Forensic Sci. Int.* **2016**, *265*(8), 107.
- [18] C. Guillou, F. Reniero, L. J. Vicente, M. Holland, K. Kolar, H. Chassaing, S. Tirendi, H. Schepers, *Curr. Pharm. Biotechnol.* **2018**, *19*, 91.
- [19] E. D. Tsochatzis, G. Giannopoulos, J. A. Lopes, C. Guillou, *Safety Science* **2021**, *137*, 105126.
- [20] J. Calvo-Castro, A. Guirguis, E. G. Samaras, M. Zloh, S. B. Kirton, J. L. Stair, *RSC Adv.* **2018**, *8*, 31924.
- [21] J. Calvo-Castro, A. Guirguis, M. Zloh, J. L. Stair, **2018**, 257.
- [22] C. Weyermann, Y. Mimoune, F. Anglada, G. Massonnet, P. Esseiva, P. Buzzini, *Forensic Science International* **2011**, *209*, 21.
- [23] J. Omar, B. Slowikowski, C. Guillou, F. Reniero, M. Holland, A. Boix, *J. Raman Spectrosc.* **2019**, *50*, 41.
- [24] L. E. Jones, A. Stewart, K. L. Peters, M. McNaul, S. J. Speers, N. C. Fletcher, S. E. J. Bell, *Analyst* **2016**, *141*, 902.
- [25] A. Guirguis, S. Giroto, B. Berti, J. L. Stair, *Forensic Science International*. <https://doi.org/10.1016/j.forsciint.2017.01.027>
- [26] L. Elie, M. Elie, G. Cave, M. Vetter, R. Croxton, M. Baron, *J. Raman Spectrosc.* **2016**, *47*, 1343.
- [27] S. Assi, A. Guirguis, S. Halsey, S. Fergus, J. L. L. Stair, *Anal. Methods* **2015**, *7*, 736.
- [28] E. Gerace, F. Seganti, C. Luciano, T. Lombardo, D. Di Corcia, H. Teifel, M. Vincenti, A. Salomone, *Drug and Alcohol Review* **2019**, *38*, 50.
- [29] S. Metternich, S. Fischmann, S. Münster-Müller, M. Pütz, F. Westphal, T. Schönberger, M. Lyczkowski, S. Zörnlein, C. Huhn, *Forensic Chem.* **2020**, 100241. <https://doi.org/10.1016/j.forc.2020.100241>
- [30] United Nations Office on Drugs and Crime. (UNODC), Guidelines on Raman handheld field identification devices for seized material, **2017**.
- [31] A. Braz, C. S. Silva, A. C. Peixoto, M. F. Pimentel, G. Pereira, P. C. C. S. Braga, A. L. Martini, T. L. F. Alcântara, *J. Raman Spectrosc.* **2021**, *52*, 901.
- [32] M. Zloh, E. G. Samaras, J. Calvo-Castro, A. Guirguis, J. L. Stair, S. B. Kirton, *RSC Adv.* **2017**, *7*, 53181.
- [33] A. D. Becke, *Phys. Rev. A* **1988**, *38*, 3098.
- [34] A. D. Becke, *J. Chem. Phys.* **1993**, *98*, 5648.
- [35] C. T. Lee, W. T. Yang, R. G. Parr, *Phys. Rev. B* **1988**, *37*, 785.
- [36] Y. Shao, L. F. Molnar, Y. Jung, J. Kusmann, C. Ochsenfeld, S. T. Brown, A. T. B. Gilbert, L. V. Slipchenko, S. V. Levchenko, D. P. O'Neill, R. A. DiStasio Jr., R. C. Lochan, T. Wang, G. J. O. Beran, N. A. Besley, J. M. Herbert, C. Y. Lin, T. Van Voorhis, S. H. Chien, A. Sodt, R. P. Steele, V. A. Rassolov, P. E. Maslen, P. P. Korambath, R. D. Adamson, B. Austin, J. Baker, E. F. C. Byrd, H. Dachsel, R. J. Doerksen, A. Dreuw, B. D. Dunietz, A. D. Dutoi, T. R. Furlani, S. R. Gwaltney, A. Heyden, S. Hirata, C.-P. Hsu, G. Kedziora, R. Z. Khalliulin, P. Klunzinger, A. M. Lee, M. S. Lee, W. Liang, I. Lotan, N. Nair, B. Peters, E. I. Proynov, P. A. Pieniazek, Y. M. Rhee, J. Ritchie, E. Rosta, C. D. Sherrill, A. C. Simmonett, J. E. Subotnik, H. L. Woodcock III, W. Zhang, A. T. Bell, A. K. Chakraborty, D. M. Chipman, F. J. Keil, A. Warshel, W. J. Hehre, H. F. Schaefer III, J. Kong, A. I. Krylov, P. M. W. Gill, M. Head-Gordon, *Phys. Chem. Chem. Phys.* **2006**, *8*, 3172.
- [37] A. Szabo, N. S. Ostlund, *Modern Quantum Chemistry: Introduction to Advanced Electronic Structure Theory*, McGraw-Hill. **1989**.
- [38] F. Jensen, *Introduction to computational chemistry*, John Wiley and sons, New Jersey, United States **2007**.
- [39] The National Institute of Standards and Technology (NIST), *Computational Chemistry Comparison and Benchmark Database, Release 21*, The National Institute of Standards and Technology (NIST) **2020**.
- [40] G. Behonick, K. G. Shanks, D. J. Firchau, G. Mathur, C. F. Lynch, M. Nashelsky, D. J. Jaskierny, C. Meroueh, *J. Anal. Toxicol.* **2014**, *38*, 559.
- [41] K. Kądzioła-Długołęcka, O. Frączak, B. Tkacz-Szczęsna, I. Kijewska, R. Wilczek, K. Makowski, P. Komorowski, R. Bachliński, A. Trynda, B. Walkowiak, *2021*, *53*, 154.
- [42] T. Breindahl, P. Hindersson, A. Kimergård, *Toxicology Communications* **2020**, *4*(1), 55.
- [43] D. Luethi, K. E. Kolaczynska, L. Docci, S. Krähenbühl, M. C. Hoener, M. E. Liechti, *Neuropharmacology* **2018**, *134*, 4.
- [44] S. Daily, **2014**.
- [45] R. V. Moreira, J. L. da Costa, M. R. Menezes, D. L. A. de Faria, *Vib. Spectrosc.* **2016**, *87*, 104.
- [46] H. Muhamadali, A. Watt, Y. Xu, M. Chisanga, A. Subaihi, C. Jones, D. I. Ellis, O. B. Sutcliffe, R. Goodacre, *Front. Chem.* **2021**, *7*, 412. <https://doi.org/10.3389/fchem.2019.00412>
- [47] C.-M. Liu, L. Xu, H.-Y. He, W. Jia, Z.-D. Hua, *Journal of Forensic Sciences* **2021**, *66*, 365.

## SUPPORTING INFORMATION

Additional supporting information may be found in the online version of the article at the publisher's website.

**How to cite this article:** J. Calvo-Castro, S. N. Tchakounte, V. Guarino, A. A. Ahmed, J. L. Stair, *J Raman Spectrosc* **2022**, *1*. <https://doi.org/10.1002/jrs.6372>